Yeganeh, Maryam; Rabensteiner, Samuel; Karimkashi, Shervin; Cheng, Qiang; Kaario, Ossi; Larmi, Martti

Experimental and Numerical Study of a Low-Pressure Hydrogen Jet under the Effect of Nozzle Geometry and Pressure Ratio

Published in:
SAE Technical Papers

DOI:
10.4271/2023-01-0320

Published: 11/04/2023

Document Version
Peer-reviewed accepted author manuscript, also known as Final accepted manuscript or Post-print

Experimental and numerical study of a low-pressure hydrogen jet under the effect of nozzle geometry and pressure ratio

Author, co-author (Do NOT enter this information. It will be pulled from participant tab in MyTechZone)

Affiliation (Do NOT enter this information. It will be pulled from participant tab in MyTechZone)

Abstract

Hydrogen (H_2), a potential carbon-neutral fuel, has attracted considerable attention in the automotive industry for transition toward zero-emission. Since the H_2 jet dynamics play a significant role in the fuel/air mixing process of direct injection spark ignition (DISI) engines, the current study focuses on experimental and numerical investigation of a low-pressure H_2 jet to assess its mixing behavior. In the experimental campaign, high-speed z-type schlieren imaging is applied in a constant volume chamber and H_2 jet characteristics (penetration and cross-sectional area) are calculated by MATLAB and Python-based image post-processing. In addition, the Unsteady Reynolds-Averaged Navier-Stokes (URANS) approach is used in the commercial software Star-CCM+ for numerical simulations. The H_2 jet dynamics is investigated under the effect of nozzle geometry (single-hole, double-hole, and multiple-hole (5-hole)), which constitutes the novelty of the present research, and pressure ratio (PR = injection pressure (P_i) / chamber pressure (P_{ch})). The results show that the H_2 jet from the single-hole nozzle possesses the fastest penetration and smallest cross-sectional area. On the contrary, the H_2 jet from the double-hole nozzle possesses the slowest penetration and largest cross-sectional area. The H_2 jet from the multiple-hole nozzle shows characteristics between those of the single-hole and double-hole. Overall, since higher pressure ratio and larger jet cross-sectional area lead to higher uniformity of the fuel/air mixture, high-pressure injection with the double-hole nozzle seems more advantageous to attain efficient mixing.

1. Introduction

Due to the current controversy in the automotive industry over the future of internal combustion engines (ICEs), extensive effort is required to evaluate possible future fuels. H_2 can serve as a promising future fuel for transition toward carbon neutrality through numerous benefits. First, green H_2 production from renewable resources such as biomass and waste gasification, biomass fermentation, hydro, wind, or solar power are entering the operation phase [1][2][3]. Second, H_2 possesses unique chemical and physical properties that significantly affect running future ICEs. For instance, H_2's wide flammability limit in the air (4-76 vol%) can provide the possibility of lean combustion, to not only reach higher thermal efficiency but also avoid drawbacks i.e., engine knocking and NOx emissions at high temperatures. Furthermore, H_2's high specific energy density can contribute to producing more energy by mass because of its great lower heating value (119.7 MJ/kg). Additionally, H_2 is light molecule and highly diffusive which assists in fast dispersion and efficient mixture formation. There are, nonetheless, major concerns with H_2's unique chemical and physical properties which need to be addressed, as well. As an example, the low density of H_2 (0.089 kg/m^3) owing to its low molecular weight (2.016 g/mol) can cause storage issues, especially in on-road applications due to the limited space in vehicles. Moreover, although H_2 has a high auto-ignition temperature (858 K), it is easily vulnerable to both pre-ignition and knocking because of its extremely low ignition energy (0.02 mJ). Another challenge is the low quenching distance (0.64 mm) along with the high flame propagation speed (1.85 m/s) which can result in backfire and combustion heat loss. However, with the possibility of retrofitting engines, introducing future H_2 ICEs can be comparatively simple [4][5][6][7][8], provided that we perform a comprehensive investigation on different H_2 combustion modes to gain further insights into the optimal design parameters.

Based on the injection strategy, combustion modes of the H_2 ICEs can be categorized in either port fuel injection (PFI) or direct injection (DI) type. Considering the above-mentioned concerns, DI application with the spark ignition (SI) is more favorable because it can offer a higher output power by a longer fuel circuit from the inlet to the exhaust and better volumetric efficiency compared to the PFI [9][10][11][12]. The other advantages of DI are preventing backfire into the intake manifold and the possibility of a cold-rated spark to minimize H_2 diffusion to hot spots and subsequently engine knocking [13][14]. However, a deeper understanding of fuel/air mixing in the DI concept is of high significance because H_2 is a low density fuel with weak tendency to transfer the momentum to the surrounding air which might cause challenges in delivering the required amount of fuel into the cylinder [15][16]. As fuel/air mixing mainly relies on the global gas jet characteristics [9][11], i.e., penetration and cross-sectional area, identifying the influential factors on the gas jet behavior can play a vital role in achieving an optimized, efficient, and low-emission combustion in H_2 DISI engines.

With relevance to the presented preface, the current study investigates the behavior of a low-pressure H_2 jet under the effect of nozzle geometry (single-hole, double-hole, and multiple-hole (5-hole)) and pressure ratio (PR). The nozzle geometry i.e., single-hole or multiple-hole can act as a prominent parameter in mixture formation through its great impact on the jet characteristics. In addition, the PR defines the rate of expansion of the compressed H_2 jet into the chamber and sets the borderline between the subsonic and supersonic flow. At supersonic injection, which is the case in the present work, the flow inside the nozzle becomes choked, and the mass flow remains constant [17][18]. Increasing PR also promotes turbulence and mixing, which is a principal target in DI engines [19]. Taking these points into account, the main objectives of the current study can be listed as:

1) experimental and numerical calculation of the H_2 jet characteristics i.e., penetration and cross-sectional area
2) comparing the experimental and numerical results of the H_2 jet characteristics to validate the simulation method
3) assessing the effect of nozzle geometry (single-hole, double-hole, and multiple-hole (5-hole)) on the H_2 jet parameters and mixing
4) assessing the effect of the pressure ratio (PR) on the H_2 jet behavior and mixing by changing the chamber pressure (P_{ch}) at a constant injection pressure (P_i).

2. Experimental methodology

This section describes the experimental setup, visualization method, image post-processing, test matrix, and experiments' error analysis, respectively.

2.1 Experimental setup

The experimental setup is a constant volume chamber with optical access through lateral windows as it is shown in Figure 1. The chamber is connected to a nitrogen bottle rack to be pressurized and to a H_2 bottle connected to the injector through the injection line. The injector is a solenoid outwardly opening gas injector from BOSCH with three different caps (single-hole, double-hole, and multiple-hole (5-hole)) with the same mass flow rate, constant injection pressure (P_i = 25 bar), and constant charge voltage of 35v. As it is shown in Figure 1, except for the single-hole nozzle, in the double-hole and multiple-hole cases, holes are not parallel to the injector axis. Following that, there is a control system (LabVIEW software and driver from National Instrument [20]) for (1) synchronizing the injector, high-speed camera (Phantom V2012), and laser light source (CAVILUX Smart laser C006, 640nm), and (2) controlling and monitoring the injection pressure (P_i), chamber pressure (P_{ch}), and temperature. Lastly, there is an exhaust line including: (1) a regulating valve to match the chamber pressure with the gas supply, (2) a shut-off valve to empty the chamber, and (3) a relief valve for releasing the pressure when reaching the maximum chamber pressure.

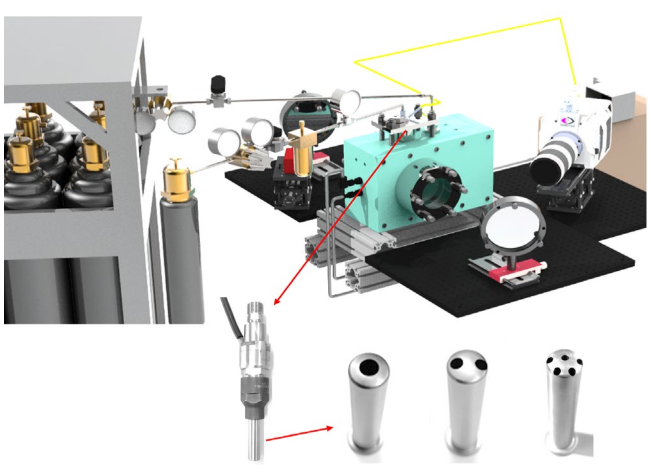

Figure 1. Experimental setup, injector, and injector's caps.

2.2 Visualization method

In the present work, high-speed z-type schlieren imaging is applied for visualizing the H_2 jet. The schlieren system operates based on bending of the light rays while facing density differences [21]. Therefore, the density difference between the H_2 jet and the surrounding (chamber filled with nitrogen) enables visalization of the H_2 jet. Figure 2 shows a schematic of the schlieren imaging system where first, the jet is illuminated by a laser light beam and the first parabolic mirror. Then, the jet refracts the light, and the second parabolic mirror concentrates the beam into the lens of the high-speed camera which is behind a schliere (iris or knife edge) for partly blocking the refracted light to generate the schlieren image. It should be also noted that due to the safety issues associated with the high chamber pressures, the injector is mounted on top of the chamber and visualization is through the quartz lateral windows which might reduce the image quality [21]. However, it is tried to overcome this concern in image post-processing by means of background subtraction.

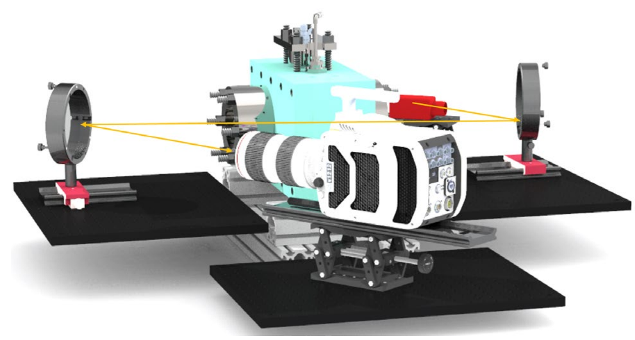

Figure 2. Schematic of the z-type schlieren imaging system.

2.3 Image post-processing

Image post-processing is carried out by developing a MATLAB code that follows the steps shown in Figure 3 to calculate the jet characteristics (penetration and cross-sectional area). As it can be observed, first, the code converts the raw image to a magnitude image. Then, it subtracts the background of the magnitude image by means of an average of the empty frames which are captured before the start of injection. After that, the code generates the binary image and denoises it to remove the shadows and small objects. Finally, based on a selected threshold value, the code traces the boundaries of the jet and presents the mean value of the jet characteristics (penetration and cross-sectional area) as the results. Another custom code is also developed in Python for structural similarity index metric (SSIM) calculation between 20 repetitions of each test point. The SSIM is almost 83% in the worst case which reveals the sufficient accuracy of the experimental data for validating CFD simulations.

Figure 3 also defines the jet penetration and cross-sectional area which are calculated through image post-processing. As it is shown, the jet penetration is the distance along the injector axis to the tip of the jet and the jet cross-sectional area is the area within the jet boundaries. It should be also mentioned that the jet penetration is calculated until the time that the jet just reaches the bottom of the chamber. Therefore, the penetration length is the same for all the cases while the penetration time is different.

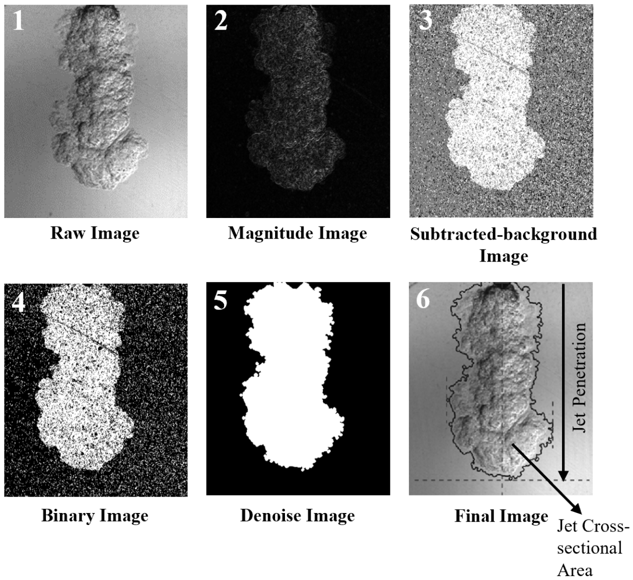

Figure 3. Steps of image post-processing in MATLAB.

2.4 Test matrix

The experimental test matrix is shown in Table 1. The measurements are performed in the room temperature (300 K) and pressure (1 atm) and as mentioned earlier, the main variables are the nozzle geometry (single-hole, double-hole, and multiple-hole (5-hole)) and PR (25, 10, 5, 2.5) which is varied by changing the chamber pressure (P_{ch} = 1, 2.5, 5, 10 bar) at constant injection pressure (P_i = 25 bar).

Table 1. Experimental test matrix (grey rows show the cases that are also investigated in the URANS simulations)

Variable	Nozzle Geometry	PR	P_i / (bar)	P_{ch} / (bar)
Case 1	Single-hole (SH)	25	25	1
		10	25	2.5
		5	25	5
		2.5	25	10
Case 2	Double-hole (DH)	25	25	1
		10	25	2.5
		5	25	5
		2.5	25	10
Case 3	Multiple-hole (MH)	25	25	1
		10	25	2.5
		5	25	5
		2.5	25	10

2.5 Experiments' error analysis

The origins of error in the current experiments can be listed as below:

1) The jet-to-jet variation which is maximum 17% based on the image similarity analysis in Python. The error bars on the jet parameters plots also show the difference between the minimum and maximum jet-to-jet variation in the results section.

2) Image post-processing in MATLAB which calculates the jet penetration and cross-sectional area up to 95% of the maximum jet penetration.

3) The injection and chamber pressure gauges with ± 0.5% of full-scale output accuracy.

4) At least 1 bar pressure drop before the injector valve during the injection and some internal pressure losses just before the nozzle e.g., in the space between the valve and the cap.

3. Methodology of CFD simulations

The commercial software Star-CCM+ is applied for Unsteady Reynolds-Averaged Navier-Stokes (URANS) simulations of supersonic H_2 jets. The URANS approach is selected based on the industrial application and limited computational time. The model utilizes a segregated flow solver and the k-ω SST Menter turbulence model, which have been previously tested and validated by the authors [22], through comparisons with high-resolution LES simulations of N_2 jets by Vuorinen et al [23]. Figure 4 (a) shows different measurements of the same jet penetration length of a single-hole H_2 jet in a constant volume chamber. The high Reynolds number flow and the supersonic shock structures can be well represented for nozzle PRs ranging from 2 to 8.5. Furthermore, a mesh-dependency study has been conducted in [22], with five different mesh resolutions in the near nozzle region ranging from 2 cells to 32 cells per nozzle diameter, which indicates that a grid resolution of at least 8 cells per nozzle diameter is required in the near nozzle region to capture the shock structure and the jet development. The convergence of the mesh-dependency study towards the LES results for the minimum jet temperature and the maximum Mach number is shown in Figure 4 (b).

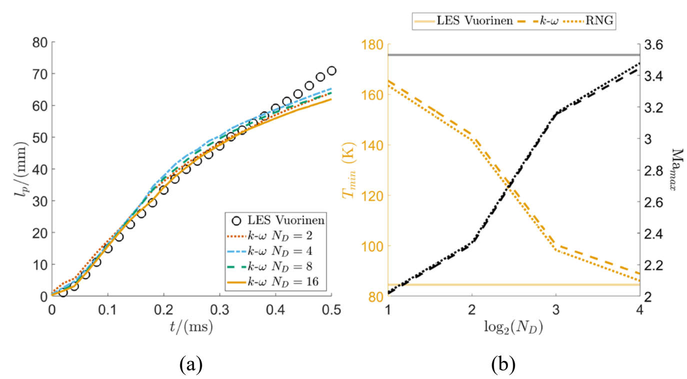

Figure 4. (a) The penetration length (l_j) for PR = 4.5 for different mesh resolutions (2, 4, 8 and 16 cells per nozzle diameter (N_D)) in comparison with LES results. (b) The minimum jet temperature (T_{min}) and the maximum Mach number ($\mathrm{Ma}_{\mathrm{max}}$), which are indicators of the supersonic jet region, converge towards the LES results for both the k-ω SST and the RNG k-ϵ turbulence model [22].

The Redlich-Kwong real gas law, as e.g., in [24], is used to account for the compressibility of the gas. More details on the solvers and turbulence models can also be found in [22]. A schematic of the simulation domain is shown in Figure 5. For simplicity, the chamber volume is chosen as a cylinder with the same height as the constant volume chamber in the experiments.

Since the simulation of the exact internal geometry of the whole injector would require significant computational power because the characteristic scales of the injector are orders of magnitude smaller than those of the chamber, a simplified injector model seems appropriate for the present case. There are several approaches for simplification e.g., the application of a boundary condition just before the nozzle hole [25] or at the location of the Mach disk (the normal shock after the nozzle exit due to the supersonic flow) [26] and simulating a region close to the injector with a high fidelity LES approach, which can then be applied as a boundary condition for simulation of the whole domain [24][27]. In the present case, a single-hole, double-hole, or multiple-hole (5-hole) nozzle cap is used on top of a hollow cone injector, and the inlet boundary is set just before the hollow cone nozzle to capture the flow in the cap. Figure 6 shows the pressure boundary for the single-hole cap.

Figure 5. The simulation domain is a simple cylinder, with the same height and volume as the experimental chamber and the injector is located at the top-center.

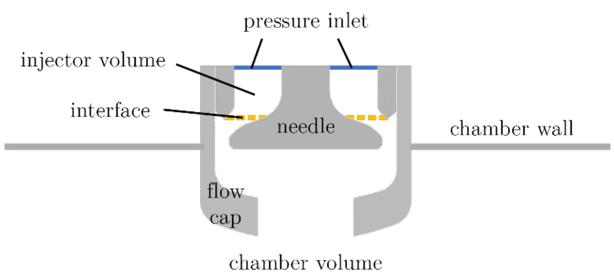

Figure 6. The pressure boundary for modelling the transient valve opening and closing of the hollow cone injector [4].

This injector model has been previously presented by the authors in [4]. In preliminary attempts, it was found that the double-hole and multiple-hole (5-hole) caps are not well represented by two or respectively five separate single holes because the complex flow inside the injector cap leads to jet-to-jet interactions, which would be neglected in such a setup. The mentioned effects can also enhance the turbulence and greatly influence the mixing of the injected gas. In addition, the valve opening and closing of the hollow cone nozzle is modelled by ramping the pressure at the inlet up and down, which represents a simplification compared to explicit modelling of the valve movement [4].

A mesh resolution in the near nozzle-exit region of 16 cells per nozzle diameter (16/D) is used for all the simulation cases. An additional refinement is also added in the hollow-cone nozzle (before the flow cap), to guarantee a mesh resolution of at least 6 cells in the orifice for all three injector cap setups. Furthermore, static cell refinement is added in cone-shaped regions for every nozzle, where the H_2 jets are expected to develop. Initially the injector is filled with H_2 up until the hollow-cone nozzle orifice, while the chamber domain is filled with ambient static air (23% mass of oxygen and 77% mass of nitrogen) at 300 K. Table 2 provides more details on the simulation setup condition.

Table 2. The simulation setup parameters

Parameter	SH	DH	MH
Nozzle diameter / mm	5	3.6	2.25
Cells per nozzle diameter in the near nozzle region	16	16	16
Minimum size of cells / mm	0.16	0.23	0.14
Total number of cells (rounded to thousands)	671000	1836000	1784000
Chamber temperature / K	300	300	300
Injection temperature / K	300	300	300
Chamber pressure / bar	2.5 & 5	2.5 & 5	2.5 & 5
Injection pressure / bar	25	25	25

4. Results and discussion

This section provides the results of the experimental campaign versus CFD simulations. First, section 4.1 presents the H_2 jet evolution from different nozzle geometries (single-hole, double-hole, and multiple-hole (5-hole)). Then, the nozzle geometry effect on the H_2 jet penetration and cross-sectional area is explained in section 4.2. After that, section 4.3 describes the effect of PR on the jet characteristics. This section is then sum up with the uniformity analysis in the simulations because the experimental results are only qualitative results based on grayscale schlieren images, and quantification is necessary for mixture formation analysis.

4.1 Jet structure development

As the main purpose of this study is to compare the H_2 jet characteristics between the experiments and simulations from different nozzle geometries, first, it is focused on the jet structure development with time progress. Figure 7 shows the H_2 jet from single-hole, double-hole, and multiple-hole (5-hole) nozzle through consecutive time frames both in the experiments and simulations at PR=10. According to this figure, the single-hole jet penetrates fastest, while the double-hole jet develops more in a radial direction. For the double-hole case, the two jets separate well, which could help to spread H_2 more uniformly throughout the chamber. Multiple-hole jet also penetrates faster than the double-hole, yet slower than the single-hole. Moreover, while the jets from different holes are separated in the near nozzle area, they seem to recombine further downstream leading to a jet development closer to a single jet and less spread in the radial direction. These observations are quantified in the following sections by comparing the geometrical development of the jet from the different nozzle layouts both experimentally and numerically. However, except for the jet penetration and cross-sectional area, other effective parameters i.e., the mixture uniformity can be quantified only through the simulations because the schlieren imaging, which is the focus of the current study, cannot provide the fuel concentration field. For experimental fuel concentration and mixture formation studies, PLIF (planar laser-induced fluorescence) measurements are recommended.

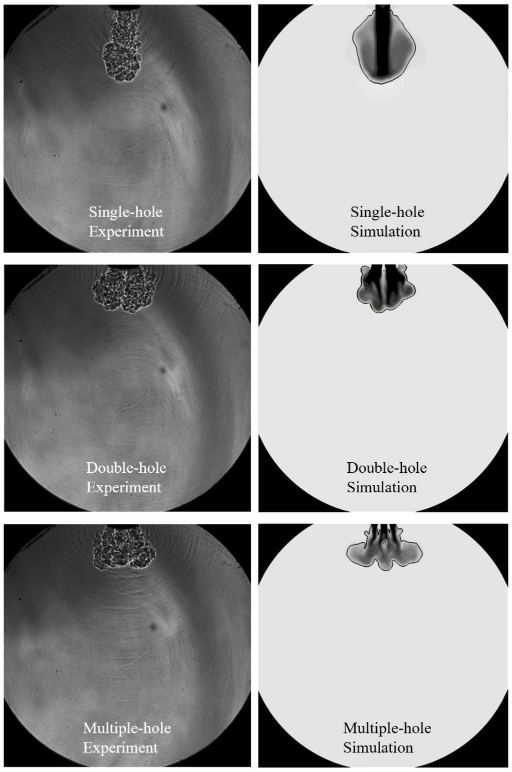

(a) $t_1 = 0.1824$ ms

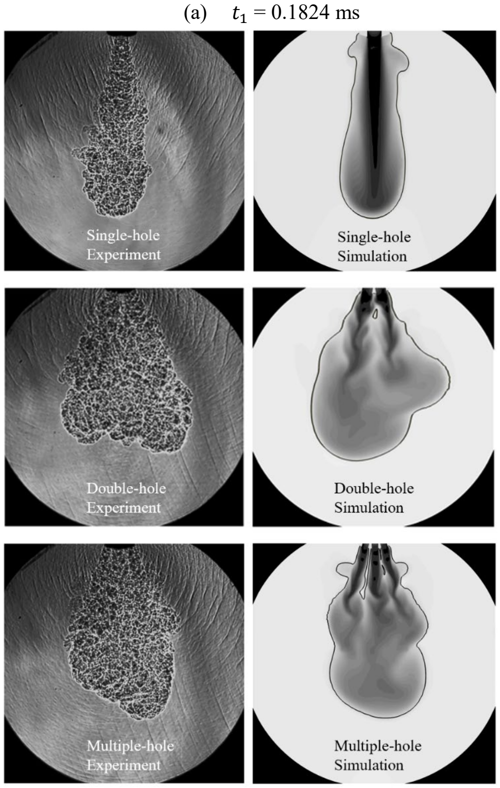

(b) $t_2 = 0.4471$ ms

Figure 7. The jet evolution from different nozzle geometries at PR = 10 within consecutive time frames with the interval of 0.2647ms. The outline of the jets from the simulations represents the threshold of 0.1 % H_2 mass fraction and the density gradient field (arbitrary scale) is shown in the background.

4.2 Effect of the nozzle geometry

This section presents the a comparison on jet characteristics from the three different nozzle layouts. As noted earlier, for this comparison, a cap, with a single-hole, double-hole or multiple-hole (5-hole), is installed on the same injector with hollow-cone outwardly opening nozzle. Figure 8 illustrates the jet penetration and cross-sectinal area versus time at PR=10 for single-hole, double-hole and multiple-hole (5-hole), separately. In accordance with this figure, there is maximum 10% discrepancy between the experiments and simulation results which indicates that the applied CFD model offers sufficiently accurate results.

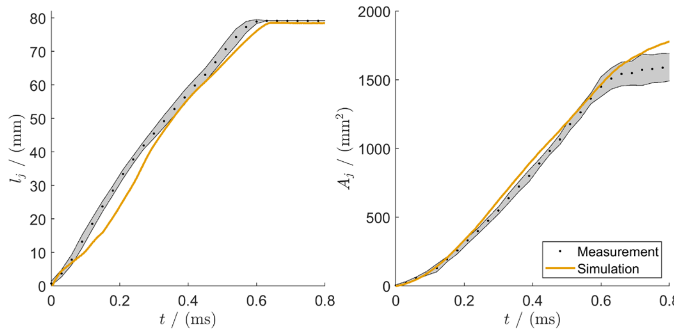

(a) single-hole

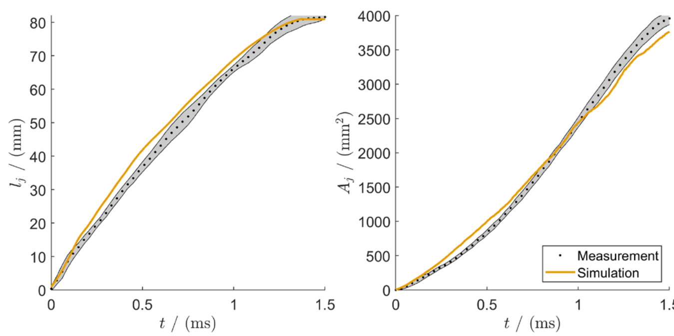

(b) double-hole

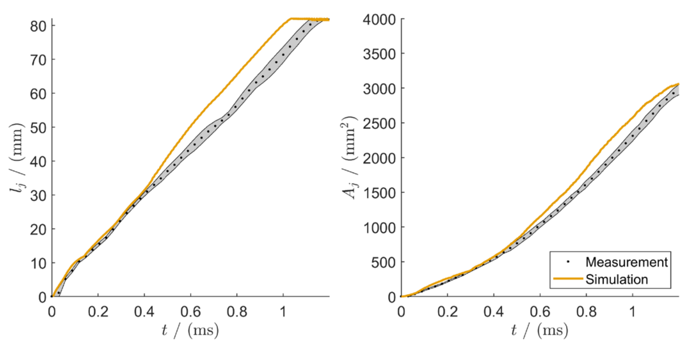

(c) multiple-hole

Figure 8. Comparison of the jet penetration and cross-sectional area in the experiments (measurement) versus simulation at PR=10 for (a) single-hole, (b) double-hole, and (c) multiple-hole (5-hole) jets.

To show the effect of the nozzle geometry on the jet characteristics more precisely, Figure 9 also demonstrates the jet penetration and cross-sectional area for single-hole (SH), double-hole (DH), and multiple-hole (MH) nozzle with time evolution. Apart from the adequate consistency between the experiments (a) and simulations (b), this figure clearly displays the fastest penetration and smallest cross-sectional area of the single-hole jet. On the contrary, the double-hole jet possesses the slowest penetration and largest cross-sectional area and the multiple-hole jet has characteristics between those of the single-hole and double-hole. Thus, based upon the fact that the double-hole jet possesses at least 10% larger cross-sectinal area, which is a dominant factor in efficient fuel/air mixing, the obvious outcome is that better mixing is estimated for the double-hole nozzle geometry.

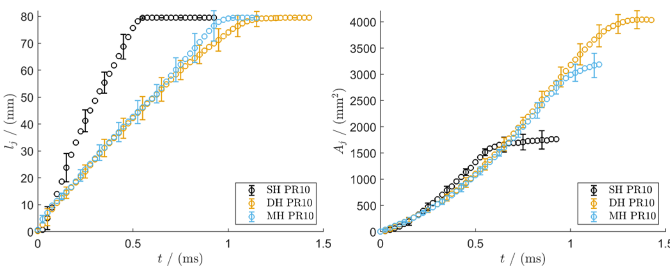

(a) experimental results

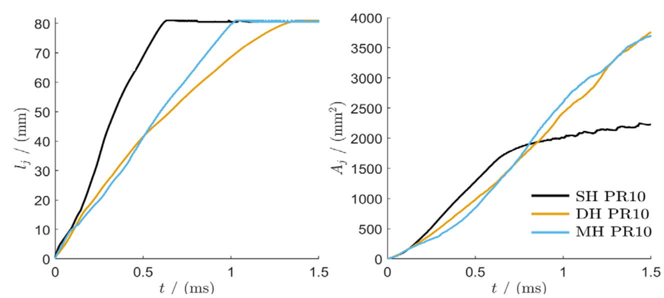

(b) simulation results

Figure 9. A comparison of single-hole (SH), double-hole (DH), and multiple-hole (MH) jet penetration and cross-sectional area from the (a) experiments and (b) simulations.

4.3 Effect of the pressure ratio (PR)

PR is the ratio of the injection pressure to the chamber pressure (P_i / P_{ch}) which highly influence the jet characteristics as it places the limit between the subsonic and supersonic flow. In the present work, the PR exceeds the limit for the choked flow meaning that the flow is supersonic for all the test points and the mass flow is constant. PR is also an effective parameter in mixture formation. Figure 10 shows the effect of PR on the H_2 jet penetration and cross-sectional area for the single-hole, double-hole and multiple-hole jet, separately. As it can be observed, higher PRs lead to faster expansion of the pressurized H_2 jet into the chamber. Therefore, higher velocities after the inlet and accordingly faster penetration at constant injection pressure are expected. Considering the constant injection pressure, higher PRs stand for lower chamber pressures where there is reduced drag against the jet expansion which enhances the H_2 jet penetration. In addition, the most effectual jet characteristic in mixing, which is the jet cross-sectional area, increases as a function of the PR.

As the final discussion, the prime outcome of the current study, which is quantifications on the effect of both nozzle layouts and PR on the mixture uniformity, is introduced via the uniformity analysis from the simulations during the injection process. Figure 11 presents a constructive insight into the effect of nozzle geometry and PR on the present H_2 jet mixing behavior. Although higher PR leads to larger jet volume [4], this is not the case for the different nozzles where all display identical development of the jet volume. Because of the design of the injector with the same effective nozzle area for all three caps and the same injection rate, the development of the equivalence ratio is almost the same for all three nozzle layouts at a given PR. Therefore, the higher uniformities for the double-hole and multiple-hole jet, during the free jet development phase, cannot be explained by better macroscopic spread of the jet in the chamber but rather by better mixing of the air and fuel inside the jet.

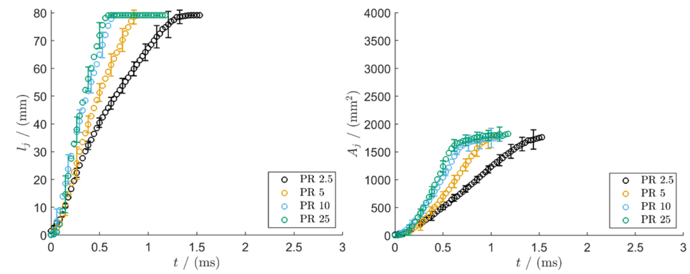

(a) single-hole

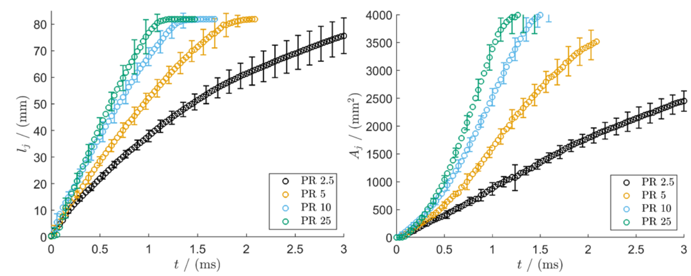

(b) double-hole

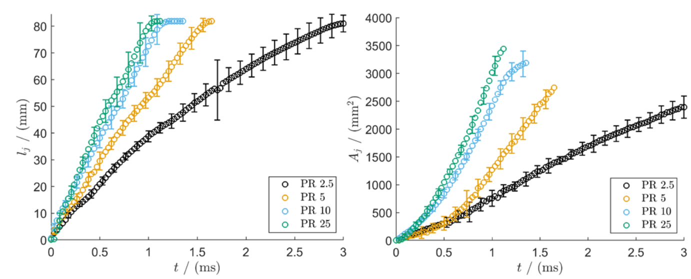

(c) multiple-hole

Figure 10. Experimental results of the effect of PR on the jet penetration and cross-sectional area for (a) single-hole, (b) double-hole, and (c) multiple-hole jets.

It is suggested that the better mixing is caused by higher turbulence levels inside the jet especially because of the jet-to-jet interactions. While the single-hole jet has a clear density gradient from the jet core to the jet edge, for double-hole and multiple-hole, this clear distinction of a core is only observed in the near nozzle area (Figure 7). Conversely, further downstream, the density is much more uniform and even the jet-to-jet interactions can be observed.

Altogether, the principal finding is that injecting a H_2 jet from the double-hole nozzle and at higher PRs can contribute to a better mixing, due to the turbulent jet-to-jet interactions and faster jet development. The presented results can also assist in selection and future development of optimized nozzle geometries that can provide efficient mixing. Here the keynote is that flow caps with more than one nozzle hole and appropriate spacing between the holes can be used to achieve jet-to-jet interactions, while still allowing for targeting the fuel to specific regions in the combustion chamber, which would be difficult to reach with a single-hole nozzle.

However, the optimized penetration time (fast enough penetration) is also of high prominence because the jet-piston interaction is another important source of turbulent mixing. Thus, further research on the effect of flow cap design, regarding the afore-mentioned issues is highly recommended and one logical next step would be to continue similar investigations both experimentally and numerically with an optical engine and a moving piston setup.

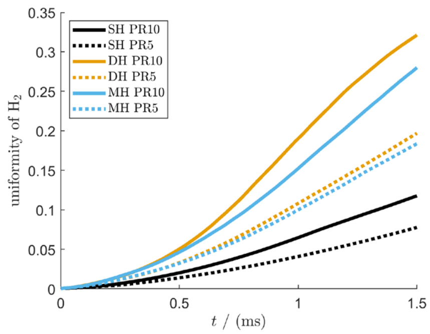

Figure 11. Effect of nozzle geometry (single-hole (SH), double-hole (DH), and multiple-hole (MH)) and PR on the volume uniformity of the H_2 mass fraction.

5. Conclusions

This paper presents an experimental and numerical (URANS simulation) investigation of a low-pressure H_2 jet dynamics to assess its mixing behavior for future design of H_2 DISI engines. The H_2 jet penetration length and cross-sectional area are studied under the effect of nozzle geometry (single-hole, double-hole, and multiple-hole (5-hole)) and PR (25, 10, 5, and 2.5). The main conclusions can be listed as:

1) There is a good consistency between the experiments and simulations which shows the appropriate accuracy of the URANS simulation approach. However, the pressure inlet condition could be improved to even better represent the early stages of the jet development. Mesh refinement could be also advanced to adaptive mesh to reduce the total amount of cells and increase accuracy in the most relevant regions, with the highest velocities and density gradients. Different PRs can be simulated for each injector cap, as well.

2) The single-hole jet shows the fastest jet penetration, followed by the multiple-hole and double-hole case. In contrast, the double-hole jet shows better jet separation and development in the radial direction compared to the single-hole and multiple-hole jets leading to higher uniformity of the fuel/air mixture.

3) The jet-to-jet interactions for the double-hole and multiple-hole nozzles, leads to a better mixing inside the jet, while the macroscopic spread of the jet in the chamber (the jet volume) is the same for all cases.

4) In the matter of application i.e., in a DISI engine, considering other influential factors such as how early the fuel injection is in the intake stroke might lead to evaluate the multiple-hole nozzle as the optimized option since H_2 possesses high diffusivity and the multiple-hole jet be can act as a good compromise between the penetration time and cross-sectional area.

5) Increasing the PR, which is the ratio of the injection pressure to the chamber pressure (P_i / P_{ch}), leads to an increase in the jet penetration and cross-sectional area. Higher PR can also assist in turbulent mixing leasing to higher mixture uniformity which is of high significance in many engine applications.

CRediT authorship contribution statement

Maryam Yeganeh: Investigation, Software, Formal analysis, Visualization, Writing – original draft, Writing – review & editing. Samuel Rabensteiner: Conceptualization, Software, Visualization, Writing - original draft Writing - review & editing. Shervin Karimkashi: Resources, Writing – review & editing. Qiang Cheng: Conceptualization, Investigation, Software, Supervision, Writing – review & editing. Ossi Kaario: Resources, Supervision, Writing – review & editing. Martti Larmi: Supervision, Funding acquisition, Writing – review & editing.

References

1. Yip, H.L., Srna, A., Yuen, A.C.Y., Kook, S., Taylor, R.A., Yeoh, G.H., Medwell, P.R., Chan, Q.N., "A Review of Hydrogen Direct Injection for Internal Combustion Engines: Towards Carbon-Free Combustion," *Applied Sciences* 9, no. 22: 4842, 2019, https://doi.org/10.3390/app9224842.

2. Cornell, A., "Hydrogen production by electrolysis", In Proceedings of the 1st International Conference on Electrolysis, Copenhagen, Denmark, 13–15 June 2017.

3. "Hydrogen Enabling a Zero Emission Europe: Technology Roadmaps Full Pack", Hydrogen Europe, Brussels, Belgium, 2018.

4. Yeganeh, M., Rabensteiner, S., Cheng, Q., Ranta, O. et al., "Experimental and Numerical Investigation of Hydrogen Jet-Wall Impingement," SAE Technical Paper 2022-01-1009, 2022, https://doi.org/10.4271/2022-01-1009.

5. Natarajan, S., Abraham, M., Rajesh, M., Subash, G. et al., "DelHy 3W - Hydrogen Fuelled Hy-Alfa Three Wheeler," SAE Technical Paper 2013-01-0224, 2013, doi:10.4271/2013-01-0224.

6. Huyskens, P., Van Oost, S., Goemaere, P., Bertels, K. et al., "The technical implementation of a retrofit hydrogen PFI system on a passenger car," SAE Technical Paper 2011-01-2004, 2011, doi:10.4271/2011-01-2004.

7. Iwasaki, H., Shirakura, H., and Ito, A., "A Study on Suppressing Abnormal Combustion and Improving the Output of Hydrogen Fueled Internal Combustion Engines for Commercial Vehicles," SAE Technical Paper 2011-01-0674, 2011, doi:10.4271/2011-01-0674.

8. Dennis, P., Dingli, R., Abbasi Atibeh, P., Watson, H. et al., "Performance of a Port Fuel Injected, Spark Ignition Engine Optimised for Hydrogen Fuel," SAE Technical Paper 2012-01-0654, 2012, doi:10.4271/2012-01-0654.

9. Yeganeh, M., Cheng, Q., Dharamsi, A., Karimkashi, S., Kuusela-Opas, J., Kaario, O., Larmi, M., "Visualization and comparison of methane and hydrogen jet dynamics using schlieren imaging," Fuel, Volume 331, Part 1,2023,125762, ISSN 0016-2361, https://doi.org/10.1016/j.fuel.2022.125762.

10. Yu, J., Vuorinen, V., Kaario, O., Sarjovaara, T., Larmi, M., "Visualization and analysis of the characteristics of transitional underexpanded jets", International Journal of Heat and Fluid Flow, 2013,44: 140–154, https://doi.org/10.1016/j.ijheatfluidflow.2013.05.015.

11. Wang, X., Sun, B., Luo, Q., Bao, L., Su, J., Liu, J., Li, X., "Visualization research on hydrogen jet characteristics of an outward

opening injector for direct injection hydrogen engines", Fuel 2020;280:118710, https://doi.org/10.1016/j.fuel.2020.118710.
12. Sankesh, D., Petersen, P., Lappas, P., "Flow characteristics of natural-gas from an outward-opening nozzle for direct injection engines,"Fuel, 2018;218:188–202, https://doi.org/10.1016/j.fuel.2018.01.009.
13. Duan, J., Liu, F., Sun, B., "Backfire control and power enhancement of a hydrogen internal combustion engine," International Journal of Hydrogen Energy, 2014;39(9):4581–9, https://doi.org/10.1016/j.ijhydene.2013.12.175.
14. Luo, Q.H., Sun, B.G., "Inducing factors and frequency of combustion knock in hydrogen internal combustion engines," International Journal of Hydrogen Energy, 2016;41(36):16296–305.
15. Kuensch, Z., Schlatter, S., Keskinen, K., Hulkkonen, T., Larmi, M., Boulouchos, K., "Experimental Investigation on the Gas Jet Behavior for a Hollow Cone Piezoelectric Injector," SAE Technical Paper 2014;01:2749, https://doi.org/10.4271/2014-01-2749.
16. Abraham, J., Magi, V., MacInnes, J., Bracco, F., "Gas Versus Spray Injection: Which Mixes Faster?," SAE Technical Paper 940895, 1994, https://doi.org/10.4271/940895.
17. Yu, J., Vuorinen, V., Hillamo, H., Sarjovaara, T., Kaario, O., Larmi, M., "An Experimental Study on High Pressure Pulsed Jets for DI Gas Engine Using Planar Laser-Induced Fluorescence," SAE Technical Paper 2012;01:1655, https://doi.org/10.4271/2012-01-1655.
18. Perry, R.H., Green, D.W., "Perry's chemical engineers' handbook", 8th ed, New York, McGraw-Hill, 2007.
19. Sakellarakis, V., Vera-Tudela, W., Doll, U., Ebi, D., Wright, Y., Boulouchos, K., "The effect of high-pressure injection variations on the mixing state of underexpanded methane jets," International Journal of Engine Research, 2021;22(9):2900-2918, https://doi.org/10.1177/1468087420960895.
20. "ni. What Is LabVIEW?," https://www.ni.com/fi-fi/shop/labview.html#, 2022 [accessed 3 May 2022].
21. Settles, G.S., "Schlieren and Shadowgraph Techniques Visualizing Phenomena in Transparent Media," 1st ed, Berlin, Heidelberg: Springer;2009, https://doi.org/10.1007/978-3-642-56640-0.
22. Rabensteiner, S., "Modelling of supersonic hydrogen jets," M.Sc. thesis, Mechanical Engineering Department, Aalto University, 2021.
23. Vuorinen, V., Yu, J., Tirunagari, S., Kaario, O. et al., "Large-eddy simulation of highly underexpanded transient gas jets," Physics of Fluids 25(1):016101, 2013, doi:10.1063/1.4772192.
24. Deshmukh, A. Y., Falkenstein, T., Pitsch, H., Khosravi, M. et al., "Numerical Investigation of Direct Gas Injection in an Optical Internal Combustion Engine," SAE International Journal of Engines, 11(6):1447–1478, (2018), doi:10.4271/2018-01-0171.
25. Keskinen, K., Kaario, O., Nuutinen, M., Vuorinen, V. et al. "Mixture formation in a direct injection gas engine: Numerical study on nozzle type, injection pressure and injection timing effects," Energy, 94:542–556, 2016, doi:10.1016/j.energy.2015.09.121.
26. Mather, D.K., and Reitz, R.D., "Modeling the Effects of Auxiliary Gas Injection on Diesel Engine Combustion and Emissions", SAE Technical Paper 2000-01-0657, 2002, doi:10.4271/2000-01-0657.
27. Deshmukh, A. Y., Vishwanathan, G., Bode, M., Pitsch, H. et al., "Characterization of Hollow Cone Gas Jets in the Context of Direct Gas Injection in Internal Combustion Engines,". SAE Technical Papers 2018-01-0296, 2018, doi:10.4271/2018-01-0296.

Contact Information

Maryam Yeganeh, M.Sc.
Doctoral Researcher
Aalto University
School of Engineering
Department of Mechanical Engineering
Research Group of Energy Conversion
Mail: P.O.Box 14300, FI-00076 Aalto, Finland
Visiting address: Sahkomiehentie 4, 02150 Espoo
Phone: +358505747731
e-mail: maryam.yeganeh@aalto.fi

Acknowledgments

This work was supported by the AGCO power company as a preliminary stage in developing a hydrogen heavy-duty engine. Special thanks to M.Sc. Olli Ranta, M.Sc. Otto Blomstedt, Senior Technician Jarno Järvinen and B.Sc. Juho Kuusela-Opas for technical assistance and mechanical design. The authors want to acknowledge the computational resources provided by the Aalto Science-IT project for performing the simulation and to thank the Triton team for their advice.

Definitions/Abbreviations

DISI	Direct Injection Spark Ignition
PR	Pressure Ratio
$\mathbf{P_i}$	Injection Pressure
$\mathbf{P_{ch}}$	Chamber Pressure
ICE	Internal Combustion Engine
PFI	Port Fuel Injection
DI	Direct Injection
CFD	Computational Fluid Dynamics
URANS	Unsteady Reynolds Averaged Navier Stokes
SSIM	Structural Similarity Index Metric